

The effect of spatial variability on the 3D slope stability evaluation

Lihang Hu^{1*} and Kiyonobu Kasama²

^{1,*}Corresponding author. Master student, Tokyo Institute of Technology, Tokyo, Japan. Email: lihang.h.aa@m.titech.ac.jp

²Associate Professor, Tokyo Institute of Technology, Tokyo, Japan. Email: kasama.k.ab@m.titech.ac.jp

Abstract: This paper presents a probabilistic slope stability evaluation considering the 3D spatial variation of soil properties by the Random Field Limit Equilibrium Analyses (simplified Bishop). Specifically, 3D random fields of cohesion, friction angle and soil unit weight were generated using the Fast Fourier transform. The Random Field Limit Equilibrium method was applied to evaluate effects of 3D spatial variability of soil property on the slope stability and failure mechanism. A Monte Carlo simulation was used to interpret the slope reliability and the variation on the collapsed slope dimension. Finally, the reliability for 3D slope with spatial variation in soil property was compared with those for 2D slope obtained from prior study.

Keywords: 3D slope stability, limit equilibrium analysis, Monte Carlo method, reliability.

1. Introduction

The spatial variability in soil property such as shear strength is well known as an inherent nature of soil and geotechnical uncertainties (Phoon & Kulhawy, 1999). The spatial variability of soil property has an influence on soil behavior such as slope stability, in order to consider the soil spatial variability in slope reliability and risk assessment, the probabilistic theory and statistic have been used. Lumb (1970) reported that the soil strength fit a normal distribution, and Kasama & Whittle (2015) used a log-normal distribution and 2D spatial variability modeling for the soil strength and performed the reliability design for 2D slope stability based on the Numerical Limit Analyses (NLA) and Monte Carlo iteration. However, as pointed out by Griffiths & Marquez (2007), the safety factor for a 2D slope is generally less than that for 3D slope, and yields conservative estimate for slope stability evaluation. Therefore, it is necessary to investigate 3D slope reliability particularly with both 3D slope stability analysis and 3D spatial variability modeling for soil property.

This paper presents a Random Field Limit Equilibrium Analysis (RFLEA) to evaluate the 3D slope stability by incorporating the spatial variability of soil property within the limit equilibrium analysis. The RFLEA is applied to evaluate effects of spatial variability of soil property on the 3D slope stability and the failure mechanism. Then a Monte Carlo simulation is used to interpret the slope reliability and the variation on the collapsed slope dimension. Finally, the reliability for 3D slope with spatial variation in soil property was compared with those for 2D slope obtained from prior study.

2. Random Field Limit Equilibrium Analysis

2.1 Limit Equilibrium Analysis (LEA)

Currently, 2D limit equilibrium analysis such as Bishop's simplified method (Bishop, 1955) and Janbu's simplified method (Janbu et al., 1956), are the most popular approaches used to evaluate slope stability. To account for the 3D geometry on slope stability, Hovland (1977), Hungr (1987) and Lam & Fredlund (1993) proposed 3D Limit Equilibrium Analysis extending simplified

Bishop's and Morgenstern and Price 2D limit equilibrium slice methods.

In this study, the Limit Equilibrium Analysis is carried out by Scoops3D, which is a computer program to evaluate slope stability using a digital landscape represented by a digital elevation model (DEM). The program uses a simplified Bishop to 3D, Scoops3D solutions are assumed by the spherical trial surface with the global minimum factor-of-safety (F). One of the advantages of this method is computational efficiency compared with other analysis methods such as 3D-FEM. For this advantage, statistical interpretation by Monte-Carlo simulation is able to carry out for 3D space.

Fig. 1 demonstrates a DEM model slope for the inclination angle of 30° . There is a soil base layer with depth $d/H = 1.0$, the horizontal long $l/H = 5.0$ and the width $w/H = 5.0$, where H is the height of the slope. Fig. 1 also illustrates the spatial distribution of shear strength and soil unit weight for each cubic element with 1.0 m resolution, as one realization with the input parameter of mean friction angle $\mu_{\tan\phi} = 0.5774$ (corresponding to 30°), mean cohesion $\mu_c = 100$ kPa and mean soil unit weight $\mu_\gamma = 20$ kN/m³. The detail input parameters are summarized in Table 1.

2.2 Random field model

The spatial variability can be modelled as a random field proposed by Vanmarcke (1977). In current study, the spatial variability of shear strength, $\tan\phi$ and c , and soil unit weight, γ , are simulated as a homogeneous random field, and assumed to have an underlying log-normal distribution with mean, $\mu_{\tan\phi}$, μ_c and μ_γ , and coefficient of variation (COV). The COV of soil unit weight (COV_γ) of the slope is fixed constant as 0.1. An isotropic scale of fluctuation, referred to as the correlation length, $\theta = \theta_{\tan\phi} = \theta_c = \theta_\gamma$ is assumed. Following Kasama & Whittle (2015) the current analysis presents the numerical result based on assumed the ratio between the correlation length and slope height, $\Theta = \theta_{\tan\phi}/H = \theta_c/H = \theta_\gamma/H$ as an input parameter.

The random field of shear strength and soil unit weight are assigned an approximately lognormal distribution. The mean and standard deviation of $\ln\tan\phi$, $\ln c$ and $\ln\gamma$ are obtained as follows:

$$\mu_{\ln \tan \phi} = \ln \mu_{\tan \phi} - \frac{1}{2} \sigma_{\ln \tan \phi}^2; \quad \sigma_{\ln \tan \phi} = \sqrt{\ln(1 + \sigma_{\tan \phi}^2)}, \quad (1)$$

$$\mu_{\ln c} = \ln \mu_c - \frac{1}{2} \sigma_{\ln c}^2; \quad \sigma_{\ln c} = \sqrt{\ln(1 + \sigma_c^2)}, \quad (2)$$

$$\mu_{\ln \gamma} = \ln \mu_\gamma - \frac{1}{2} \sigma_{\ln \gamma}^2; \quad \sigma_{\ln \gamma} = \sqrt{\ln(1 + \sigma_\gamma^2)}. \quad (3)$$

$\tan \phi$, c , and soil unit weight, γ , for the i th element are given as follows

$$\tan \phi_i = \exp(\mu_{\ln \tan \phi} + \sigma_{\ln \tan \phi} \cdot G_i), \quad (4)$$

$$c_i = \exp(\mu_{\ln c} + \sigma_{\ln c} \cdot G_i), \quad (5)$$

$$\gamma_i = \exp(\mu_{\ln \gamma} + \sigma_{\ln \gamma} \cdot G_i). \quad (6)$$

where G_i is a standard Gaussian random variable that is linked to the correlation length θ . Detailly, the FFT (Fast Fourier Transform) technique generates G_i that is derived from the isotropic random field G with the zero mean, one variance (normal distribution), and a Markov correlation function:

$$\rho(x_{ij}) = \exp(-2x_{ij} / \theta). \quad (7)$$

where ρ is the correlation coefficient, x_{ij} is an absolute distance from point i to point j , and θ is a correlation length.

3. Simulation Results

3.1 Stability number

The stability number N_{si} is used to evaluate the stochastic property of slope stability with the spatial variability of soil property as follows:

$$N_{si} = \frac{F_{si} \cdot \mu_\gamma \cdot H}{\mu_c}. \quad (8)$$

where N_{si} is a number for each iteration, i , F_{si} is a factor-of-safety of slope for i th iteration.

In order to evaluate the effect of spatial variability, stability number ratio R_{Ns} and mean stability number ratio $\mu_{R_{Ns}}$ are introduced as follow:

$$R_{Ns} = \frac{N_{si}}{N_{s_hom}}; \quad \mu_{R_{Ns}} = \frac{1}{n} \sum_1^n R_{Ns}. \quad (9)$$

where N_{s_hom} is the stability number for homogeneous slope with the slope angle $\beta = 30^\circ, 45^\circ$ or 60° , shear strength $\tan \phi = 0.5774$, $c = 100$ kPa, and soil unit weight $\gamma = 20$ kPa.

Fig. 2 shows a 13-bin histogram of the stability number ratio from one complete series of Monte-Carlo iterations with $COV_c = 1.0$ and $\theta = 0.25$ and 1.0 . According to the Chi-square test of goodness of fit test, a 2.5% significance level for the normal and log-normal distribution fits the stability number. Besides, Fig. 2 demonstrates that large θ results in large COV_{Ns} .

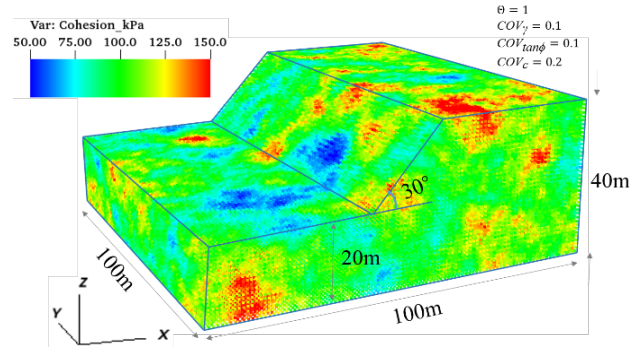


Figure 1. Model geometry and distribution of strength.

Table 1. Input parameters

| Parameter | Value |
|---|-----------------------------------|
| Angle of slope, β | $30^\circ, 45^\circ$ & 60° |
| Mean soil cohesion, μ_c | 100 kPa |
| COV of cohesion, COV_c | 0.2, 0.4, 0.6, 0.8 and 1.0 |
| Mean friction angle, $\mu_{\tan \phi}$ | 0.5774 ($\mu_\phi = 30^\circ$) |
| COV of friction angle, $COV_{\tan \phi}$ | 0.1, 0.2, 0.3, 0.4 and 0.5 |
| Mean unit weight, μ_γ | 20 kN/m ³ |
| COV of unit weight, COV_γ | 0.1 |
| Ratio of vertical and horizontal correlation length | 1 (Isotropic) |
| Normalized correlation length, $\theta = \theta_{\tan \phi} / H = \theta_{mc} / H = \theta_{m\gamma} / H$ | Random, 0.05, 0.25, 0.5 and 1.0 |
| Cross correlation coefficient between c and $\tan \phi$, $\rho_{c-\tan \phi}$ | 0.5 |
| Monte-Carlo iteration | 1000 |

Fig. 3 shows the relationships between mean stability number ratio and normalized correlation length θ for given $COV_{\tan \phi} = 0.1$ to 0.5 and $COV_c = 0.2$ to 1.0 . It can be seen that $\mu_{R_{Ns}}$ decrease with increasing θ irrespective of $COV_{\tan \phi}$ and COV_c while the decrease rate decreases as θ increase. For example, the maximum decrease in mean stability number ratio $\mu_{R_{Ns}}$ is about 14% for $COV_{\tan \phi} \& COV_c = 0.5 \& 1.0$ when θ varies from 0.05 to 0.25 .

3.2 Sliding volume

In order to evaluate on slope failure dimension, sliding volume ratio R_v and mean sliding volume ratio are introduced as follow:

$$R_v = \frac{V_i}{V_{hom}}; \quad \mu_{R_v} = \frac{1}{n} \sum_1^n R_v. \quad (10)$$

where V_i is a sliding volume for each iteration i , V_{hom} is the sliding volume for homogeneous slope.

Fig. 4 shows a histogram of the sliding volume ratio for $COV_\gamma = 0.1$, $COV_{\tan \phi} = 0.5$ and $COV_c = 1.0$ from one complete series of Monte-Carlo simulation. It is shown that the sliding volume decrease sharply for large θ . Furthermore, it can be noted that COV_{R_v} increases with increasing θ , which is suggested that sliding volume shows a large variation as θ increases.

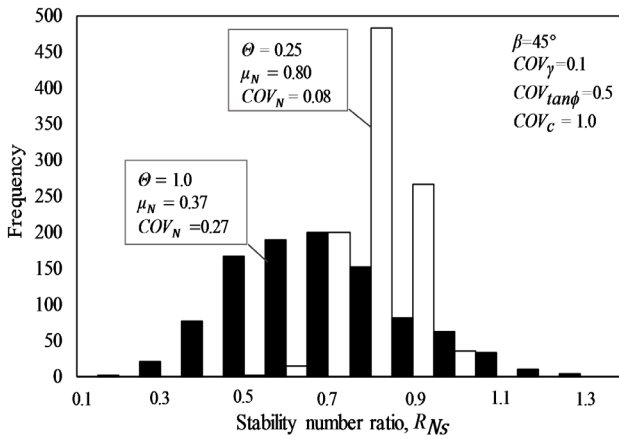


Figure 2. Histogram of stability number for slope.

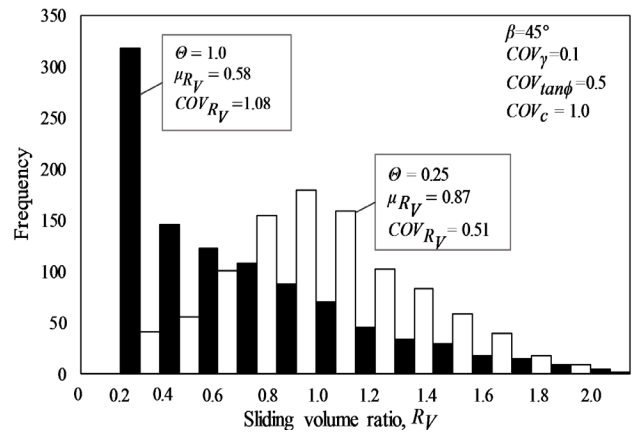


Figure 4. Histogram of sliding volume ratio.

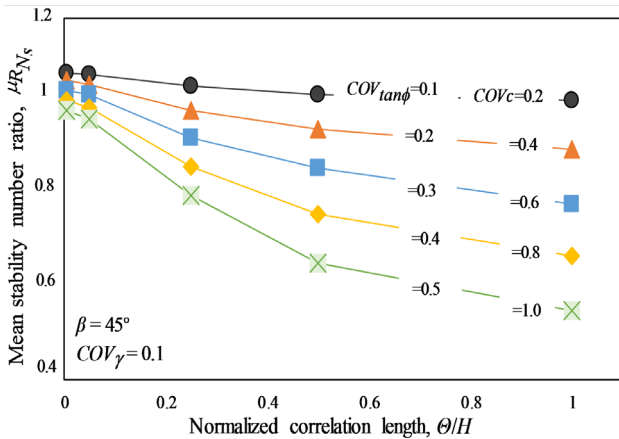


Figure 3. Mean stability number ratio and normalized correlation length.

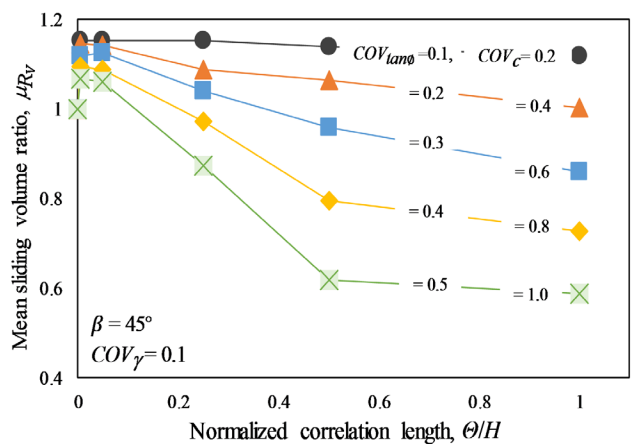


Figure 5. Mean sliding volume ratio and normalized correlation length.

Fig. 5 summarizes the mean sliding volume ratio μ_{R_V} and the normalized correlation length Θ , where the μ_{R_V} means the mean sliding volume ratio of one complete series of Monte-Carlo iteration. It demonstrates that sliding volume becomes small with increasing the COV of shear strength and Θ . However, by comparing the R_V for a given $COV_{tan\phi}$ & COV_c and Θ , it is suggested that R_V is affected by Θ rather than $COV_{tan\phi}$ & COV_c for slope angle = 45° . For instance, the decrease in μ_{R_V} is around 29% when Θ varies from 0.25 to 0.50 for a given $COV_{tan\phi}$ & $COV_c = 0.5$ & 1.0 .

3.3 Effect of slope angle

Fig. 6 presents the relationships between mean stability number μ_{N_s} for $\Theta = 1.0$ and slope angle. Note, there are two comparable results for the stability number for homogeneous strength ($COV_{tan\phi} = 0$, $COV_c = 0$ and $COV_\gamma = 0$) in this figure, the solid line refer to the results of current study, another dashed line refers to previous research from Ugai et al (1988). It can be seen that the stability number $N_{s, home}$ for homogeneous slope of 30° , 45° and 60° obtained from current study is equivalent to 14.92, 11.87 and 9.22 respectively reported by Ugai with the numerical accuracy of 2%, and the maximum difference is less than 4% for slope angle = 60° . In addition, the stability number N_s decreases linearly with

increasing of slope angle for $\Theta = 1.0$.

Fig. 7 is a histogram of stability number ratio R_{N_s} for a given slope angle with $COV_{tan\phi}$ & $COV_c = 0.5$ & 1.0 , $COV_\gamma = 0.1$ and $\Theta = 0.25$. The stability number decreases with increasing slope angle, the variability of stability number ratio becomes large when the slope angle is large.

Fig. 8 is a histogram of sliding volume ratio R_V for a given slope angle similar condition to Fig. 7. The small sliding volume is dominant for large slope angle while large sliding volume is dominant for small slope angle. It is also noted that the variation of sliding volume ratio becomes large when the slope angle is large. Therefore, from Figs. 7 and 8, it can be concluded that the variability of shear strength along the slip surface becomes large when the sliding volume becomes small with increasing slope angle, in other words, the local averaging of shear strength along the slip surface occurs and triggers local failure as increasing the slope angle.

Fig. 9 shows the relationships between mean stability number ratio R_{N_s} and sliding volume ratio R_V for $\beta = 30^\circ$, $COV_\gamma = 0.1$ and $\Theta = 0.5$. It is noted that the square range of $\mu_{R_{N_s}} \pm \sigma_{R_{N_s}}$ and $\mu_{R_V} \pm \sigma_{R_V}$ for $COV_{tan\phi}$ & $COV_c = 0.1$ & 0.2 , 0.3 & 0.6 , and 0.5 & 1.0 is shown in this figure. There is a positive correlation between the stability number ratio R_{N_s} and sliding volume ratio R_V , which

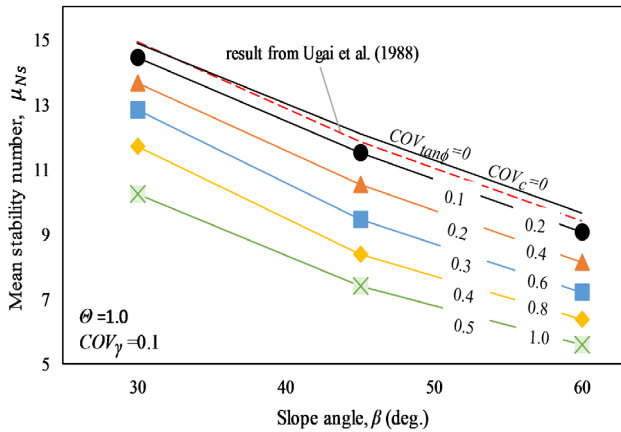


Figure 6. Mean stability number against slope angle.

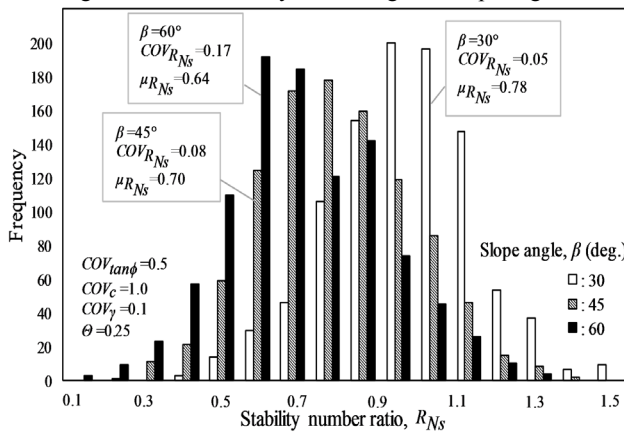


Figure 7. Histogram of stability number ratio respect of slope angle.

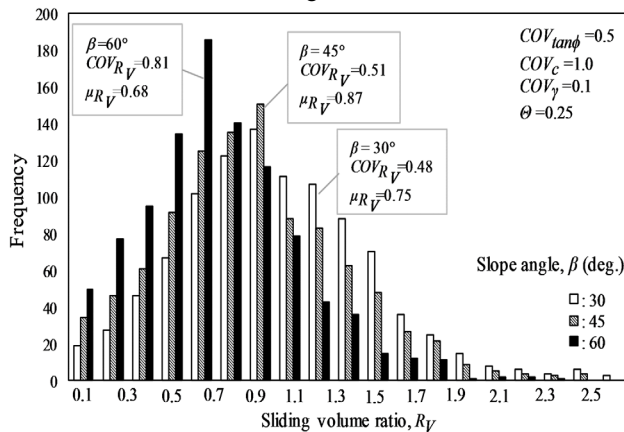


Figure 8. Histogram of sliding volume ratio respect of slope angle.

illustrates a large stability number always accompanied a large sliding volume. For the effect of the spatial variability on the R_{Ns} and R_V , it can be seen that the standard deviation of stability number ratio $\sigma_{R_{Ns}}$ is smaller than that of sliding volume ratio σ_{R_V} , which suggests that the R_V varied more significantly rather than R_{Ns} , namely the sliding volume has large variation rather than stability number.

Fig. 10 shows the mean stability number ratio $\mu_{R_{Ns}}$ against normalized correlation length θ for a given slope angle $\beta = 45^\circ$ and different combinations of

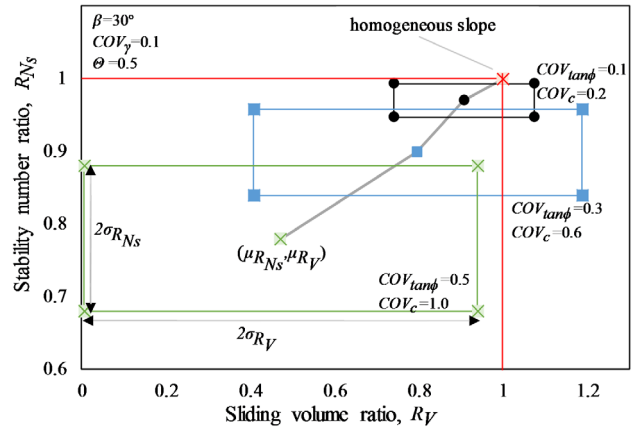


Figure 9. Mean stability number ratio and sliding volume ratio.

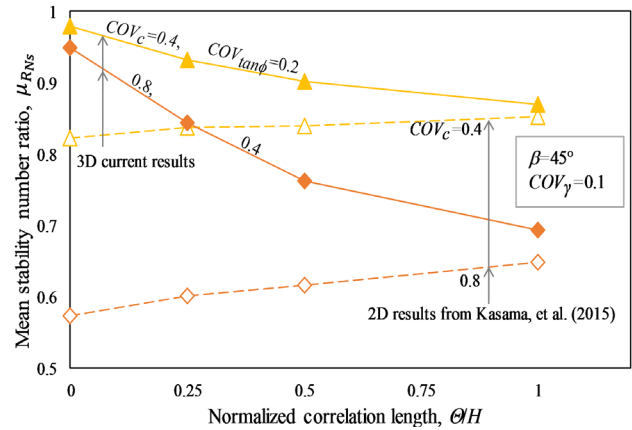


Figure 10. Mean stability number ratio and normalized correlation length considering the 2D and 3D.

$COV_{tan\phi}$ & COV_c . With regards to the dimension effect, the 2D results by Kasama & Whittle (2015) are also plotted. It is seen that the results from 2D slope are less than those from current result in 3D. It suggests that conservative result is obtained for not only homogeneous slope but also spatially varied slope. The decrease in stability number due to large spatial variability has a good consistency for 2D and 3D, however, the stability number decrease for 3D is more significant rather than that for 2D. However, the effect of correlation length on 2D and 3D is entirely different. Namely, large θ results in small N_s in 3D although large θ yields a large N_s in 2D. From author's opinion, this opposite result is because the normalized correlation length (0 ~ 1) in this study is too limited to observe the same tendency with 2D, and this effect will be conducted in future study.

3.4 Failure mechanism

In this study, the 4 failure modes were identified regarding the shape of sliding soil body. The failure mode 1 characterized as a large volume failure with the sliding volume includes slope crest and slope toe in addition to slope face. As alternative failure modes, failure mode 2 includes the slope toe and slope face while failure mode 3 includes the slope face and slope crest. For failure mode 4, its sliding volume includes

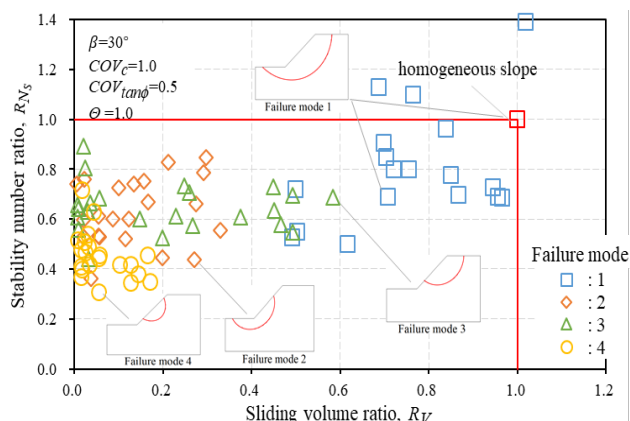


Figure 11. Failure modes on the space of R_{Ns} and R_V .

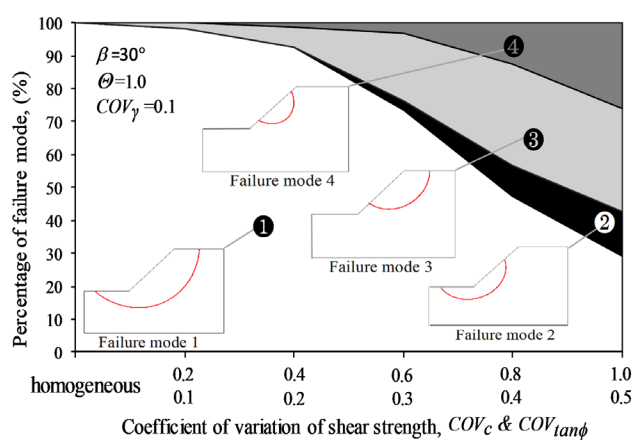


Figure 12. Percentage of failure mode against COV of shear strength.

slope face which should be expressed as a typical small and local failure.

In order to examine the failure mechanism in terms of the stability number and sliding volume, the relationship among R_{Ns} , R_V and failure mode is plotted in Fig. 11 for $\beta = 30^\circ$, $COV_{tan\phi}$ & $COV_c = 0.5$ & 1.0 and $\theta = 1.0$. It is noted that the failure mode 1 is the deterministic mode for homogeneous slope ($COV_{tan\phi}$ & $COV_c = 0$) with angle $= 30^\circ$. It can be seen that that the failure mode 1 has large possibility when R_{Ns} & R_V close to 1.0. For the failure mode 4, it is demonstrated that the values of R_{Ns} & R_V became small compared with other three modes. It is clear that small and local failure generates a small stability number and sliding volume. It is confirmed that there is a positive correlation between stability number and sliding volume for each failure mode.

In order to evaluate the probability of occurrence of each failure mode in terms of spatial variability, the percentage of failure mode against COV of shear strength and normalized correlation length are plotted in the Fig. 12 and Fig. 13.

For Fig. 12, It is noted that failure mode 1 is the deterministic mechanism for homogeneous slope ($COV_{tan\phi}$ & $COV_c = 0$), and the possibility of failure mode 1 gradually decreases as the COV of shear strength increases. On the other hand, the possibility of failure

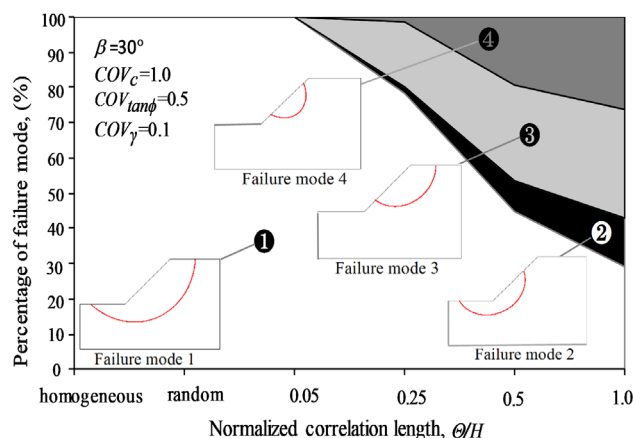


Figure 13. Percentage of failure mode against normalized correlation length.

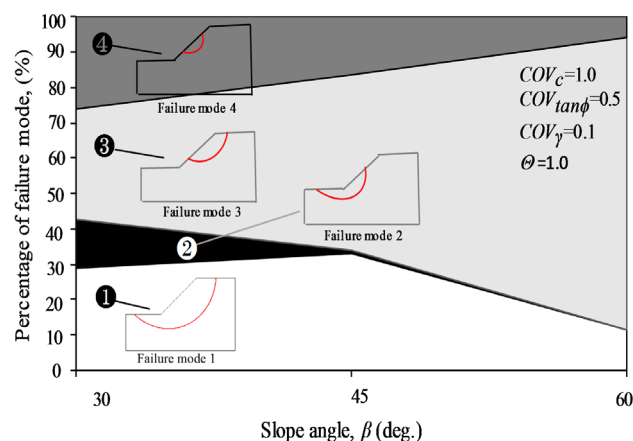


Figure 14. Percentage of failure mode against slope angle.

mode 2 to 4 gradually increases with increasing COV of shear strength. It should be pointed out that the possibility of failure mode 4 increases with increasing COV_c & $COV_{tan\phi}$, which indicates that small and local failure occurs by increasing the spatial variation of shear strength. Nevertheless, the mode 1 (varied from 100 % to 29.1 %) and mode 3 (varied from 0 % to 31.1 %) are the two primary failure modes affected by the spatial variation of shear strength. It also should be emphasized that the slope failure mechanism shows a great diversity at large $COV_{tan\phi}$ & COV_c .

For Fig. 13, it is noted that “random” in horizontal axis means the correlation of shear strength is very small that could be regarded as a “random” distribution. It should be noted that the failure mode 1 is deterministic mechanism (100% of possibility of occurrence) for homogeneous and random these two conditions, and the possibility of this failure decreases with the increasing the normalized correlation length. Besides, other three modes increase especially for mode 3 and mode 4. Similar to the effect of variation of shear strength discussed in Fig. 3, the mode 1 and mode 3 are optional failure mode caused by the change in correlation length. It also should be informed that diverse failure mode appears for large correlation length.

To evaluate the failure mechanism considering the slope inclination, Fig. 14 demonstrates the percentage of failure mode regarding slope angle for a given $COV_{\tan\phi}$ & $COV_c = 0.5$ & 1.0 and $\Theta = 1.0$. It is found that failure mode 3 becomes dominant failure mode while modes 1 and 2 gradually fade away as the slope inclination increases. It is emphasized that as the slope angle increases the failure mechanism shifts from general failure mode, which is a large sliding volume including slope toe and crest for homogeneous slope, to a local failure including slope face and crest. It should be noted that the mode 1 and mode 3, whose sliding volume include the slope crest, are become main failure mode with increasing the slope angle (total 94% at slope angle = 60°). It is clear that a failure mode including slope crest is a general failure mechanism for a steep slope. It is also found that as the slope angle decreases, the slope failure mechanism shows a great diversity. For example, in slope with angle = 30° the 4 failure modes can be found, and the possibility of these four modes are quite comparable, however for slope with angle = 60° , mode 2 is disappeared and the possibility of other three modes are also apparently different.

4. Conclusions

This paper presents a probabilistic slope stability evaluation considering the 3D spatial variation for soil property by the Random Field Limit Equilibrium Analyses and Monte Carlo simulation. The main conclusions are as follows:

- (1) A normal and log-normal distribution functions with 2.5% significance level can be used to describe the stability number of 3D slope considering the spatial variability of shear strength and unit soil weight.
- (2) The ratio of stochastic stability number normalized by that for homogeneous slope is less than 1.0, and decrease with increasing of the correlation length and the coefficient of variation in the shear strength. The maximum decrease in mean stability number ratio is about 14% for $COV_{\tan\phi}$ & $COV_c = 0.5$ & 1.0 when Θ/H varies from 0.05 to 0.25.
- (3) The sliding volume for spatially varied slope decreases with increasing the correlation length, and the variation of sliding volume increases with increasing the slope angle.
- (4) The slope crest involved failure is the general failure mechanism for a steep slope.

References

- Bishop, A.W. 1955. The Use of the Slip Circle in the Stability Analysis of Earth Slopes. *Géotechnique*, 5, 7-17.
- Morgenstern, N.R. and Price, V.E. 1965. The Analysis of the Stability of Generalised Slip Surfaces. *Géotechnique*, 15, 79-97.
- Lumb, 1970. The variability of natural soils. *Canadian Geotechnical Journal*, 3(2), 74-97.
- Hovland, H.J. 1977. Three-dimensional slope stability analysis method. *Journal of the Geotechnical Engineering Division*. 103(9), 971-986.

Vanmarcke, E.H. 1977. Probabilistic modeling of soil profiles. *Journal of the Geotechnical Engineering Division*. 103(11), 1227-1246.

Hungr, O. 1987. An extension of Bishop's simplified method of slope stability analysis to three dimensions. *Géotechnique*, 37(1), 113-117.

Ugai, K. and Hosobori, K. 1988. Extension of Simplified Bishop method, Simplified Janbu method and Spencer's method to three dimensions. *Proceedings of JSCE*. 394(9), 21-26.

Phoon, K.K. and Kulhawy, F.H. 1999. Characterization of geotechnical variability. *Canadian Geotechnical Journal*. 36, 612-624.

Griffiths & Marquez. 2007. Three-dimensional slope stability analysis by elasto-plastic finite elements. *Géotechnique*. 57(6), 537-546.

Kasama, K. and Whittle, A.J. 2015. Effect of spatial variability on the slope stability using Random Field Numerical Limit Analyses. *Georisk: Assessment and Management of Risk for Engineered Systems and Geohazards*. 10(1), 42-54.

Waled A.D; Kasama, K. et al. 2016. Statistical evaluation of geotechnical correlations. *International Journal of GEOMATE*, 10(21), 1929-1935.